RSC Advances

ARTICLE

Isatin thiosemicarbazone-blended polymer films for biomedical applications: surface morphology, characterisation and preliminary biological assessment

Received 00th January 20xx,
Accepted 00th February 20xx

DOI: 10.1039/x0xx00000x

www.rsc.org/advances

David Mallinson[a+], Polyxeni Alexiou[b+], Alexander B. Mullen[a], Maria Pelecanou[b], Marina Sagnou[b*], Dimitrios A. Lamprou[ac*]

Poly (methyl methacrylate) and polyurethane are polymers currently used for a range of biomedical applications. To modify their surface characteristics, biocompatibility and potentially reduce any related side effects the addition to the polymers of appropriate compounds has been investigated. Isatin thiosemicarbazone derivatives were synthesised and added to poly (methyl methacrylate) and polyurethane solutions before spin coating them on to a silica wafer. The resultant films were characterised with contact angle goniometry and atomic force microscopy. PMMA films produced from tetrahydrofuran solvent displayed honeycombed structures which were highly hydrophobic; however, such changes were not seen for polyurethane surfaces. The cytotoxicity and effect on cell proliferation of polymer surfaces were investigated using PNT2A prostate cells. The isatin-containing polymers were deemed non-toxic at the concentrations used, while cell proliferation studies suggested that the resulting films were supportive of cell growth.

Introduction

Implantable medical devices have revolutionised the practice of modern medicine. However, stenting procedures are often accompanied by undesirable side effects such as encrustation, inflammation and bacterial adhesion[1]. Some of these phenomena are closely related to the ability of proteins to be directly adsorbed onto the stent surface. In the case of ureteral devices, for example, the most common problems associated with indwelling are encrustation, bacterial adhesion and biofilm formation on the device surface. Encrustation is often associated with infection by urease-producing bacteria such as *Proteus mirabilis* and some *Klebsiella* species leading to increase in urinary pH, an environment that favours bacterial growth and mineral crystallisation[2]. Moreover, an implant's surface characteristics, such as hydrophobicity, roughness, porosity and chemical composition, have direct influence on the protein and bacterial adsorption and are closely associated with a variety of adverse reactions, including inflammation, fibrosis, thrombosis and infection[3]. In order to make medical implants safer, increase their biocompatibility and stave off side effects, coating with a variety of materials, ranging from diamond-like carbon[4] to heparin[5] and polymers, have been introduced. Polymers, such as poly(lactic-co-glycolic acid) (PLGA)[4], are employed as coatings for metal stents providing both the strength and durability of the metal skeleton and the tunable properties of the polymer.

Biocompatibility improvement can be achieved by introducing regular patterns on the implant surface with ordered morphologies and controllable sizes[5]. Several polymers are already being used in biomedical settings such as polyurethane (PU) for ureteral catheters[2], poly (methyl methacrylate) (PMMA)[6] for bone glue and polytetrafluoroethylene (PTFE) for vascular grafts[7] or hernia repair[8]. Most of the reported studies rely on neat polymer molecules, however, by 'blending' in pharmacologically active compounds into the polymers, surface modifications might be achieved affecting not only the biocompatibility, chemical or structural properties but also pathogen susceptibility, cell growth and cell metabolism.

Isatin (1H-indole-2,3-dione) and its derivatives have sparked great attention in recent years due to their wide variety of biological activities. Isatin was first discovered as a product of indigo oxidation[9], and has been recognised as an endogenous human biomolecule as found to be an adrenaline metabolite. It is evident from the literature that isatin derivatives are associated with a diverse range of biological activities including anti-inflammatory[10, 11], anti-nociceptive[12], antibacterial[13-20], antifouling[21], antiviral[22], and anticorrosion[23]. Despite this broad spectrum of activities, little research has been performed on

[a] Strathclyde Institute of Pharmacy and Biomedical Sciences (SIPBS), University of Strathclyde, 161 Cathedral Street, Glasgow, G4 0RE, United Kingdom
[b] NCSR 'Demokritos', Institute of Biosciences and Applications, Athens, Greece.
[c] EPSRC Centre for Innovative Manufacturing in Continuous Manufacturing and Crystallisation (CMAC), University of Strathclyde, Technology and Innovation Centre, 99 George Street, Glasgow, G1 1 RD, United Kingdom
+ Equal contribution
* Corresponding authors: sagnou@bio.demokritos.gr, dimitrios.lamprou@strath.ac.uk Tel: +44 (0)141 548 4968
DOI: 10.1039/x0xx00000x

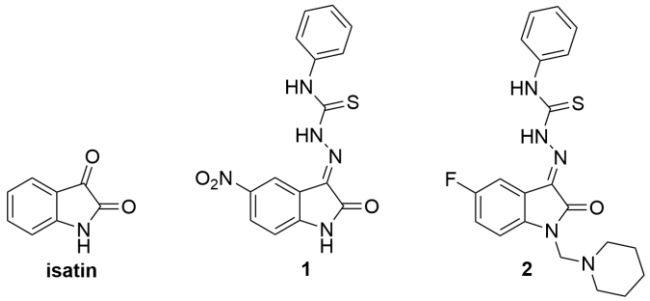

Fig. 1 Isatin and the thiosemicarbazone derivatives.

their incorporation into biomaterials. Tahermansouri and Chitgar[24] included an isatin derivative in a carbon nanotube creating a material that was highly toxic to gastric and colonic cancer cells.

It was therefore of interest to study the effect of two new isatin derivatives **1** and **2** (Fig 1) on the generation of PU and PMMA surfaces. Both derivatives share the common feature of the phenyl thiosemicarbazone moiety which is characterised by extensive electron delocalisation and it may exist in a tautomeric form, the thione and the thiol form. The 5-position of the isatin core bears an electron withdrawing substituent, either the highly polarisable nitro group (derivative **1**) or the more compact fluorine atom (derivative **2**). Derivative **1** has previously been investigated by Pervez *et al.*[25], showing some antileishmanial activity. Ali *et al.*[26, 27] has investigated the derivatives resemble compounds for anticancer/antiproliferative activities. They found that the presence of a fluorine in the position it is in derivative **2** above lowered the IC_{50} values for cytotoxicity against HCT 116 cells. These compounds were not necessarily chosen for their demonstrated activities since they are similar to structures that are biologically active. In the current study, derivative **2** the isatin NH functionality has been alkylated depriving the molecule of its capacity to hydrogen bond through this site. The PU and PMMA surfaces developed after blending in derivatives **1** and **2** were characterised by contact angle goniometry (CAG) and atomic force microscopy (AFM) and evaluated for their cell growth potential.

Experimental

Materials

Poly (methyl methacrylate) (PMMA; MW 94,600 g mol^{-1}) was purchased from Acros Organics and polyurethane (PU) from Fluka. Tetrahydrofuran (THF), toluene, ethylene glycol (EG), diiodomethane (DIM), RPMI 1640 cell culture media, L-glutamine, trypan blue and foetal bovine serum (FBS) from Sigma. Kanamycin sulphate and trypsin-EDTA from Life Technologies. RPMI 1640 complete media was made from L-glutamine (1 % v/v), kanamycin sulphate (1 % v/v) and foetal bovine serum (10 % v/v) in RPMI-1640 media. Unless otherwise stated, all reagents and solvents for the synthesis stage were obtained from Alfa Aesar or ChemBiotin and used without further purification.

Of the solvents used in this study, THF has a greater vapour pressure (19.3 kPa) than toluene (3.8 kPa), with the boiling point of THF (66 °C) being far lower than for toluene (111 °C). Moreover, THF is more hydrophilic than toluene (logP values of 0.46 and 2.73, respectively), with the density of the solvents being approximately identical for THF (0.88 g cm^{-3}) and toluene (0.86 g cm^{-3}). This information will help the reader to understand the different structures on the produced isatin-polymer blended surfaces.

Isatin derivative synthesis

Air sensitive chemical synthesis was performed in dry and inert conditions under a nitrogen atmosphere. All reactions were routinely checked by Thin-layer chromatography (TLC) on Silica gel Merck 60 F254 and compounds were purified by column chromatography on silica gel using the appropriate solvent systems or by preparative High-performance liquid chromatography (HPLC). The purity of the biological tested compounds was determined by an analytical HPLC method and was found to be greater than or equal to 95 %. The purity was determined automatically by MS parameters and was performed on a HPLC Shimadzu 2010EV (Column: Merck Purospher RP-C8, 250 x 4.6 mm, 5 µm particle size), equipped with a SPD-20A UV/Vis detector. Characterization of target compounds was established by a combination of ESI-MS and NMR spectrometry techniques. ^{1}H and ^{13}C NMR spectra were recorded on a Bruker Avance DRX spectrometer (500 MHz). Chemical shifts are presented in ppm (δ) with internal TMS standard. MS were obtained by the mass detector of the already mentioned HPLC Shimadzu 2010EV.

Isatin derivatives synthetic procedure

The thiosemicarbazones were prepared by combining equimolar amounts of the commercially available substituted isatins (3.5 mmol) and thiosemicarbazide (3.5 mmol) dissolved in ethanol followed by the addition of a few drops (100-200 µL) of glacial acetic acid to initiate the reaction. The mixture was refluxed overnight and the corresponding thiosemicarbazone precipitated during the course of the reaction. All final compounds were recrystallized from DMSO with a small amount of water.

Derivative 1 ((E)-2-(5-nitro-2-oxoindolin-3-ylidene)-N-phenylhydrazinecarbothioamide): This was synthesised according to the general procedure by reacting 5-nitroisatin with 4-phenyl-3-thiosemicarbazide. Yield = 74%. ^{1}H NMR (500Hz, DMSO-d_6) δ 12.57 (s, 1H), 11.87 (s, 1H), 11.10 (s, 1H), 8.71 (d, *J* = 2.0 Hz, 1H), 8.30 (dd, *J* = 8.7, 2.3 Hz, 1H), 7.60 (d, *J* = 7.7 Hz, 2H), 7.47 (t, *J* = 7.8 Hz, 2H), 7.32 (t, *J* = 7.3 Hz, 1H), 7.15 (d, *J* = 8.7 Hz, 1H); ^{13}C NMR (125.5 MHz, DMSO-d_6,) δ 176.50, 163.05, 147.55, 142.81, 138.28, 130.34, 128.51, 127.11, 126.44, 126.03, 120.94, 116.76, 111.28; ESI-MS (m/z) [M+H]+ calculated for [$C_{15}H_{12}N_5O_3S^+$] 342.07 Found: 342.15, HPLC analysis: peak area = 95.770 %, Mobile Phase A: aq. CH_3COONH_4 10 mM, pH=3.9 with formic acid; Mobile Phase B: MeOH; Detected at 255 nm.

Derivative 2 ((E)-2-(5-fluoro-2-oxo-1-(piperidin-1-ylmethyl)indolin-3-ylidene)-N-phenylhydrazinecarbothioamide): This was synthesised in two steps. 5-fluoroisatin initially reacted with 4-phenyl-3-thiosemicarbazide according to the general procedure. To a suspension of the resulting (E)-2-(5-fluoro-2-oxoindolin-3-ylidene)-N-phenylhydrazinecarbothioamide (2 mmol) in absolute ethanol, 37 % formaldehyde solution and piperidine (2 mmol) were subsequently added dropwise with vigorous stirring. After combining all reagents, the reaction mixture was stirred at 500 rpm at room temperature for 10 h. The solid product was filtered and washed with petroleum ether. Yield (for the two steps) = 61 %. ^{1}H NMR (500Hz, DMSO-d_6) δ 12.61 (s, 1H), 10.89 (s, 1H), 7.70 (d, *J* = 8.0 Hz, 1H), 7.62 (d, *J* = 7.6 Hz, 2H), 7.45 (t, *J* = 7.8 Hz, 2H), 7.32 – 7.28 (m, 3H), 4.50 (s, 2H), 2.56 – 2.53 (m, 4H), 1.53 – 1.42 (m, 4H), 1.39 – 1.29 (m, 2H).; ^{13}C NMR (125.5 MHz, DMSO-d_6,) 176.28, 161.75, 159.57, 157.68, 140.21, 138.25, 128.45, 126.25, 125.61, 120.74, 120.66, 117.45, 117.26, 112.57, 112.51, 108.02, 107.81 , 62.10, 51.30, 25.33, 23.53.; ESI-MS (m/z)[M+H]+ calculated for [$C_{21}H_{23}FN_5OS^+$] 412.16 Found: 412.21, HPLC analysis: peak area = 96.765 %, Mobile Phase A: aq. CH_3COONH_4 10 mM, pH=3.9 with formic acid; Mobile Phase B: MeOH; Detected at 255 nm.

Spin Coating

Polymers used as purchased from the suppliers and not prepared from monomers. Polymer solutions were made with 2 % w/v poly (methyl methacrylate) PMMA or polyurethane (PU) in tetrahydrofuran (THF) or toluene by leaving it overnight in a sealed glass vial in order to be dissolved. Isatin derivative solution (dissolved in THF to 10 mg mL^{-1}) was added to the polymer solution to provide the following preparations where isatin derivatives are used at 10 μM unless otherwise stated (Table 1). Silica wafer (SW) was cut into 100-200 mm^2 pieces and cleaned with 70 % v/v ethanol and finally with the solvent that was used in individual polymer solutions. Solutions were applied to silica wafer and spun at 2000 rpm for 30 s with a Laurell WS-400-6NPP spin coater. Humidity was measured by placing an Exoterra digital hygrometer within the spin coater on a dry run. Experiments were repeated at least 3 times on different surfaces.

Table 1 Naming of the surfaces according to isatin derivative, solvent and polymer. Derivatives used at 10 μM except for surface I which was used at 50 μM to investigate the effect of a higher concentration.

Derivative	None		Derivative 1		Derivative 2	
Polymer	PMMA	PU	PMMA	PU	PMMA	PU
THF	A	B	E, I	F	J	K
Toluene	C	D	G	H	L	M

Contact Angle Goniometry (CAG)

Surface energy (γ_s) and their components, were determined by measuring the contact angles of three solvents on surfaces. Briefly, the contact angle of drops of deionised water (DW; 18.2 MΩ, γ_L 72.8 mN m^{-1} at 20 °C), diiodomethane (DIM; γ_L 50.8 mN m^{-1} at 20 °C) and 1,2-ethanediol (ethylene glycol) (EG; γ_L 48.0 mN m^{-1} at 20 °C) (surface tension γ_L values from Lamprou *et al.* [28]) on surfaces were measured with a Krüss DSA30B contact angle goniometer. Advancing angles (θ_A) were obtained from both the left and right side of each drop at 10-20 s after drop placement. Substrate surface energies (γ_s) were then calculated from the mean contact angles using the Good and Oss 3-liquid formula [29] via an in-house Visual Basic program [28].

Atomic Force Microscopy (AFM)

AFM was performed with a Bruker Multimode 8 atomic force microscope with a Nanoscope V controller in ambient conditions in air. ScanAsyst Air probes (Bruker) with V-shaped silicon nitride cantilevers with nominal spring constants of 0.4 Nm^{-1} were used. Peak force quantitative nanomechanical mapping mode was used in air in order to scan the surface with a resolution of 512 samples per line and scan rate of 1 Hz. Roughness (Ra) data was calculated using Nanoscope Analysis on five images at scan size 5 × 5 μm.

Cytotoxicity and cell proliferation studies

PNT2A cells (prostate cells) were grown in RPMI complete media. Cells were grown at 37 °C in a 5 % CO_2 atmosphere and split when they reached 70-80 % confluence. For the cytotoxicity studies isatin derivatives were tested in solution. They were dissolved in THF (10 mg mL^{-1}) then diluted further in media and compared against solvent (THF), and media-only controls by means of an Alamar blue (resazurin) assay. The initial solutions were clearly homogeneous after dilution with media, without any precipitation during the incubation as experiments took place at 37 °C which helps increase the solubility without losing THF. Resazurin is converted to fluorescent resorufin by cells such as the fluorescence can be indicative of metabolic rate and cell population. Fluorescence was read with a SpectraMax M5 (Molecular Devices) with excitation at 560 nm and emission at 590 nm. For proliferation on surfaces cells were grown on sample surfaces at the bottom of a 24-well cell culture plate for in triplicate with an empty (polystyrene) well as a control. After 2 days' cell growth, the cell media was replaced with resazurin-cell media solution and incubated for 24 h. Then two aliquots were taken of each well and fluorescence measured as before.

Statistical Analysis

Significances for contact angles (Table 2) were found through two-sample Student's unpaired T-tests for each pair of samples within each solvent. Significances for cytotoxicity (Fig. 5) were calculated with two-sample Student's unpaired T-tests between each concentration's sample and its solvent-only equivalent control. Significances for cell proliferation (Fig. 6) were calculated with two-sample Student's unpaired T-tests between each surface and the control surface. Significance tests were performed in Minitab 17. The significance level chosen was 0.05.

Results and discussion

Synthesis

Both derivatives **1** and **2** were successfully prepared in high yield by treating the corresponding 5-substituted isatin moiety with phenyl thiosemicarbazide. The desired products precipitated out of the reaction mixture in high purity. The products are soluble in most organic solvents and give stable solutions. Based on the general structural characteristics of the two derivatives, it is anticipated that the polar THF solvent would interact more with the NH- group, the nitro-related local charge and potentially stabilise the thiol tautomeric form of derivative **1**. This could create areas of repulsion leading to a more ordered arrangement. On the contrary, this cannot be feasible for derivative **2** due to lack of the free NH- moiety and the different electronic effect of the 5-fluoro group. With regards to toluene, it could not promote any favourable arrangement for the two derivatives. With the given experimental conditions, the compounds should not interact in any direct way with the polymers.

Contact Angle Goniometry

Table 2 Advancing contact angles (θ_A) of the probe liquids (deionised water (DW), ethylene glycol (EG) and diiodomethane (DIM)) on the surfaces (n = 6) as in Table 1.

Surface	Advancing contact angles (θ_A) / °		
	DW	EG	DIM
A	77.3 ± 0.5	54.0 ± 2.5	40.7 ± 1.1
B	85.1 ± 1.1	57.9 ± 2.7	42.1 ± 7.5
C	66.5 ± 6.6	56.0 ± 1.6	38.5 ± 1.0
D	72.2 ± 1.6	46.1 ± 6.6	49.7 ± 2.3
E	118.8 ± 0.7	96.5 ± 2.7	73.0 ± 5.4
F	88.8 ± 1.8	63.9 ± 2.2	34.9 ± 1.6
J	109.6 ± 6.2	86.4 ± 8.3	69.7 ± 13.3
K	90.8 ± 1.7	70.5 ± 2.9	33.2 ± 1.3
SW	57.9 ± 10.4	34.0 ± 5.0	42.2 ± 2.6

Table 3 Surface energies (γ_s) and their components as determined by CAG, and AFM surface roughness (R_a) values. Surfaces are as described in Table 1.

Surface	γ_{s+} / mJ m^{-2}	γ_{s-} / mJ m^{-2}	γ_{sLW} / mJ m^{-2}	γ_s / mJ m^{-2}	R_a by AFM / nm
A	0.00	8.77	39.26	39.48	1.88 ± 0.33
B	0.01	4.02	38.54	38.86	19.66 ± 2.75
C	0.23	21.98	40.34	44.83	0.56 ± 0.18
D	0.41	11.18	34.42	38.73	2.20 ± 0.64
E	0.26	0.00	21.21	21.22	23.37 ± 0.99
F	0.17	3.15	42.07	43.54	21.15 ± 1.91
J	0.02	0.25	23.04	23.19	15.04 ± 1.02
K	0.74	3.67	42.85	46.14	7.02 ± 0.66
SW	0.33	22.36	38.49	43.92	0.15 ± 0.04

Advancing contact angles (θ_A) of the probe liquids on the surfaces with and without the isatin derivatives are presented in Table 2. Both compounds cause a significant increase in surface hydrophobicity, as highlighted by the increased water contact angles in the case of the THF/PMMA surfaces (from 77.3° to 118.8° for surfaces A and E). An angle of 118.8 ± 0.7° was observed for the addition of derivative **1** in 2 % w/v PMMA in THF (surface E). The lower surface energy values (Table 3) correlate well with high water contact angle values. The roughness values (Table 3) also correlate well with the water contact angle values (Table 2) as high roughness can correspond to high water contact angle as seen with the lotus effect[30] where air pockets remain under the drop giving rise to super-hydrophobicity. The AFM images of surfaces E (Fig. 3) and J (Fig. 4) show that they are rough with space for air pockets. It is likely, however, that the hydrophobicity would not persist once the air pockets collapse. There is a large difference in hydrophobicity between the PMMA-only surfaces (surfaces A and C) and those where an isatin derivative has been added to PMMA (surfaces E and J), which is associated with a large difference in surface roughness (Ra) ($p < 0.01$). It should be highlighted at this point that rougher surfaces can be favourable towards cell proliferation or osseointegration[31, 32].

Atomic Force Microscopy

The AFM images of the surfaces generated from PMMA or PU solutions in the absence of isatin derivatives **1** and **2** are shown in Fig. 2, while the images of the surfaces in the presence of **1** and **2** are given in Figs 3 and 4 respectively. Honeycombed structures were formed in both polymers (PMMA and PU) in the case of THF, but not in the presence of toluene as solvent. Toluene surfaces (Figs. 2B&D, 3B&D, 4B&D) are flat in comparison with the THF ones. The height scales in Fig. 3B and Fig. 3D are 6 nm and 12 nm respectively, while the pores in surface E (Fig. 3A) are 64.4 ± 7.3 nm deep and 312.8 ± 69.8 nm in diameter.

The presence of isatin derivatives and the use of THF as a solvent appear to have an important influence on the formation of pores. By shifting the morphology from a smooth surface (A; R_a = 1.6 ± 0.7 nm) to rough surface with a honeycomb structure

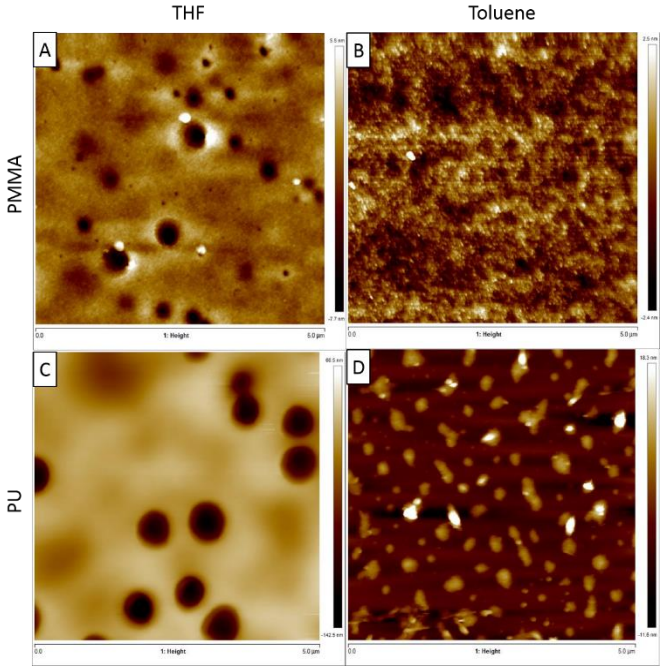

Fig. 2 AFM height images of PMMA- or PU-only surfaces cast from toluene or THF. A) Surface A; B) surface C; C) surface B; D) surface D, as described in Table 1. Images are 5 x 5 µm.

(E; R_a = 23.4 ± 1.0 nm) led to an increase in hydrophobicity as indicated by the water contact angles and surface energies (Tables 2 & 3).

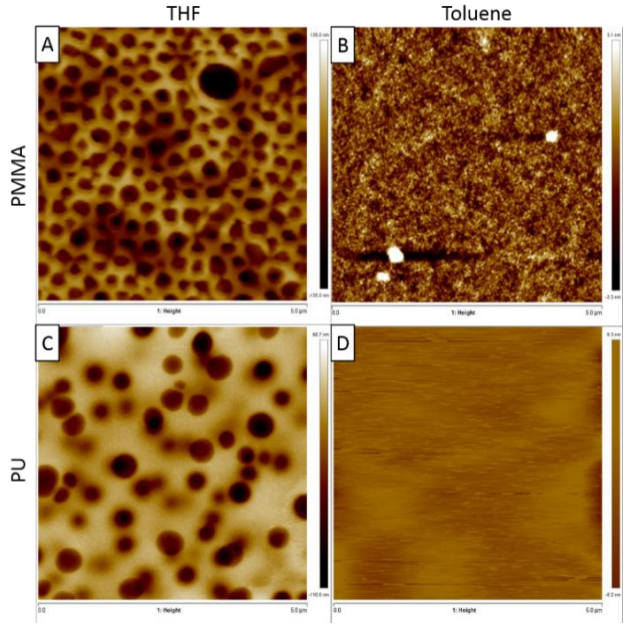

Fig. 3 AFM height images of derivative **1**-PMMA and PU surfaces made with THF or toluene. A) surface E; B) surface G; C) surface F; D) surface H, as described in Table 3. Images are 5 x 5 µm.

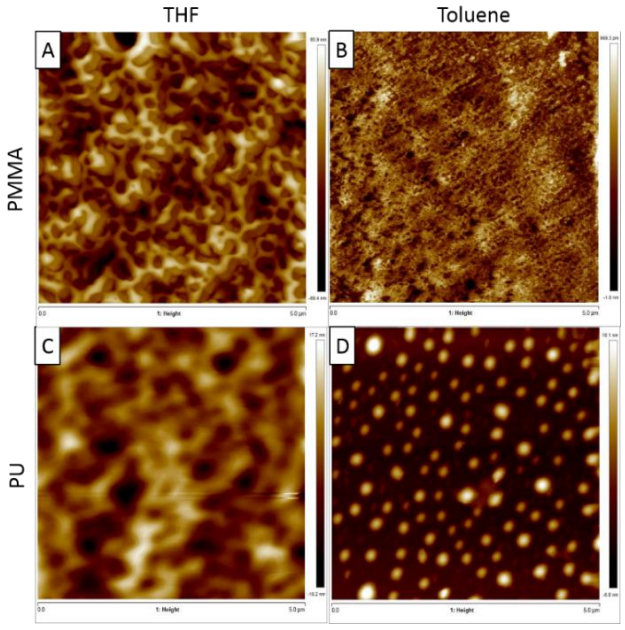

Fig. 4 AFM height images of derivative **2**-PMMA and -PU surfaces made with THF or toluene. A) surface J; B) surface L; C) surface K; D) surface M, as described in Table 3. Images are 5 x 5 µm.

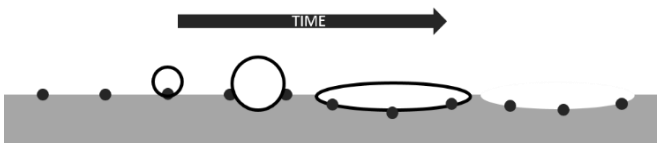

Fig. 5 Breath figure array formation process with particles (black dots). Water droplets nucleate and grow. The droplets partially sink in to the polymer surface acting as template while the solvent evaporates before evaporating themselves.

The honeycombed structures imaged by AFM (Figs. 2-4) appear to be breath figure arrays (BFAs). BFAs are formed when water droplets act as a template around which a polymer is cast, as illustrated in Fig. 5. The droplets are formed by condensation on the solvent/air interface and can sink into the surface. As the solvent evaporates the temperature can fall to 0 °C which assists water condensation[33]. The droplets grow and their packing can become ordered. A hexagonal arrangement is optimal (seen as a honeycomb) but this can be compromised if droplets are too far apart to interact or coalesce. When all the solvent has evaporated the polymer will be cast in that position and the water can evaporate[33]. Spin coating tends to give smaller pores than dip coating or drop casting because a portion of the solution is lost at the beginning of the process and the solvent evaporates faster giving less time for the droplet to grow[34].

It is evident from the AFM images that the isatin derivatives have a clear effect on the topography of the generated surfaces. With THF as a solvent, they both produce pores that in the case of derivative **1** are much more prevalent and appear well ordered. Their specific effect on BFA formation is also demonstrated by the low relative humidity (RH 20-30% ambient conditions) under which they were formed, since in the absence of polymer doping formation of BFAs requires a humidity of above 50%[29]. Jiang *et al.*[30] reported that the addition of silver nanoparticles to polyurethane films allowed BFA formation in humidity conditions of 30% where they would not otherwise form. Contamination of the THF as a solvent with water would also contribute to BFA formation as shown by Park and Kim[35] and by Jiang et al.[36], however on its own would not explain the difference between the polymer-only surfaces (Fig. 2) and the derivative-doped surfaces (Fig. 3 & 4). Comparison with data from Park and Kim suggests a water content of ≤ 2 % v/v[35].

The effect exerted by isatin derivatives may be related with their potential aggregation at the water/polymer surface forming a layer that stabilizes the condensed water droplets as has been suggested in the literature for silver[30] and gold[33], nanoparticles as well for self-organizing amphiphilic clusters[34] and self-associating organic molecules[37].

During the BFA process, the isatin derivatives may be prone to self-assembly as they possess multiple sites of intermolecular interaction potential through hydrogen bonding, π-π interactions and dipolar interactions. Such a process may explain the more ordered surfaces generated in THF by derivative **1** compared to derivative **2** which lacks the indole NH functionality and the potential for hydrogen bonding through this site. The differential behaviour of the more polar THF compared to toluene may be also related with an overall stabilisation of a potential aggregation process. Our continuing investigations on the conditions of generating new isatin-blended polymers will hopefully provide more clues on the way isatin derivatives lead to ordered structures.

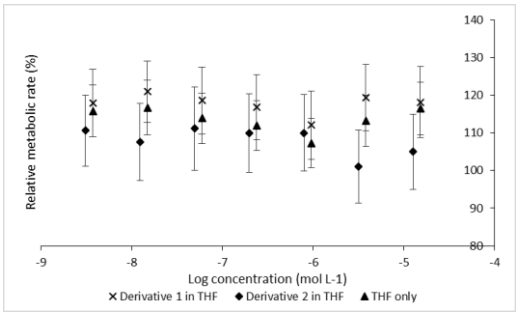

Fig. 6 Mean metabolic rate and standard deviation (indicative of cell survival, relative to cells grown in media only) for cells dosed with isatin derivatives **1** and **2**.

Cytotoxicity and Cell Proliferation

The compounds do not appear to be cytotoxic in solution at the concentrations tested relative to controls (Fig. 6). This means that if the derivatives are released from the polymers will not be harmful in the human body. THF was required because the derivatives were not water soluble, therefore was tested as a control to see if it made any changes to cell survival.

Cell proliferation data are presented in Fig. 7. Cells displayed significantly greater metabolic activity on the surface E (derivative **1**; 10 µM PMMA; THF) which suggests that increased cell growth is supported in this case. Additionally, surface E supported cell proliferation better than the control surfaces (flat polystyrene). The beneficial effect of porous topography has previously been reported with fibroblasts grown on quartz (7-25 µm diameter pores)[38], honeycombed polystyrene-polypyrrole copolymer surfaces (~1 µm diameter) [39] and titanium (~6 µm diameter)[40], and HeLa cells grown on poly(L-lactide)-poly(L-lysine) copolymer surfaces (0.9 µm diameter pores)[41]. The above reported data reveal a tendency for smaller diameter pores to offer better cell proliferation. The pores in the current study have even smaller diameters (e.g. 312.8 ± 69.8 nm in Fig. 3A) than the ones the authors are aware of being investigated for cell growth. The positive results for surface E in Fig. 7 support the idea that smaller pores can be supportive of cell growth.

Though hydrophilic surfaces, such as chitosan, heparin and polyvinylpyrrolidone (PVP) are used antibacterial surfaces[42], rough or hydrophobic surfaces have also been shown to be promising[42, 43]. While rough surfaces can be more prone to encrustation by plaque accumulation due to increased surface area for bacterial attachment[44] their low surface energy can also repel bacteria[42]. This suggests that roughness and hydrophilicity alone are not the sole determining factors for the level of encrustation or bacterial attachment.

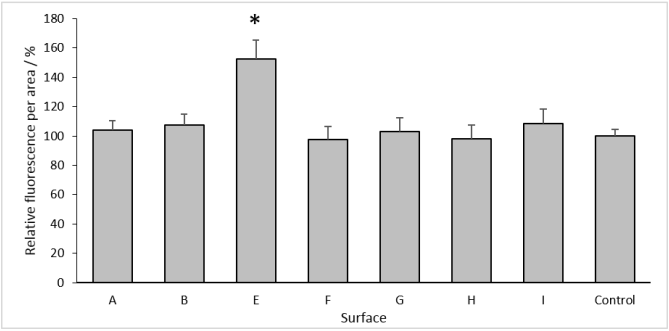

Fig. 7 Cell proliferation on surfaces as described in Table 1. Metabolism relative to control as indicated by fluorescence. * – significantly different to control and other surfaces, p <0.01. The control surface was polystyrene.

Conclusion

Despite the simple fast procedure of honeycomb film formation, several parameters can play a role in the honeycomb film morphology influencing for instance pore size or quality of ordering and cell growth. In this study, PU and PMMA films were prepared and isatin derivatives **1** and **2** were added to their solutions before spin coating on silica wafer in order to investigate the formation of honeycomb structures. The use of isatin thiosemicarbazone derivatives and tetrahydrofuran as a solvent was found to promote the formation of honeycombed structures by breath figure arrays which are known to improve biocompatibility and osseointegration. Cell proliferation studies have shown that the incorporation of derivative **1** into PMMA results in a honeycombed product with improved hydrophobicity that supports cell growth. In the current study, surface E significantly outperformed all other surfaces investigated in terms of cell proliferation which suggests that isatin derivative **1** incorporation into PMMA would be beneficial. In conclusion, the developed herein surfaces lend themselves to be used as biomaterials.

Acknowledgements

The authors would like to acknowledge the UK Engineering & Physical Sciences Research Council (EPSRC) and the University of Strathclyde for the studentship to David Mallinson, and the EPSRC Centre in Continuous Manufacturing and Crystallisation (CMAC) for access to equipment. The authors would also like to acknowledge the Hellenic Republic and the European Union as part of the European Regional Development Fund, in the context of the O.P. Competitiveness and Entrepreneurship (OPC II) and the R.O.P. Attica, R.O.P. Macedonia - Thrace, through the implementation of the program KRIPIS-DIAS, Institute of Biosciences & Applications, NCSR "Demokritos" for their financial support.

References

1. A. Al-Aown, I. Kyriazis, P. Kallidonis, P. Kraniotis, C. Rigopoulos, D. Karnabatidis, T. Petsas and E. Liatsikos, *Therapeutic advances in urology*, 2010, **2**, 85-92.
2. D. Lange and B. H. Chew, *Therapeutic advances in urology*, 2009, **1**, 143-148.
3. P. Thevenot, W. Hu and L. Tang, *Curr Top Med Chem*, 2008, **8**, 270-280.
4. M. Talja, M. Multanen, T. Valimaa and P. Tormala, *Journal of endourology / Endourological Society*, 2002, **16**, 299-302.
5. L. C. Palmer and S. I. Stupp, *Acc Chem Res*, 2008, **41**, 1674-1684.

6. J. C. J. Webb and R. F. Spencer, *Journal of Bone & Joint Surgery, British Volume*, 2007, **89-B**, 851-857.
7. A. I. Cassady, N. M. Hidzir and L. Grøndahl, *Journal of Applied Polymer Science*, 2014, **131**.
8. A. Lukasiewicz and T. Drewa, *Advances in clinical and experimental medicine : official organ Wroclaw Medical University*, 2014, **23**, 135-142.
9. G. Mathur and S. Nain, *Medicinal Chemistry*, 2014, **4**, 417-427.
10. P. D. Fernandes, R. S. Zardo, G. S. Figueiredo, B. V. Silva and A. C. Pinto, *Life sciences*, 2014, **116**, 16-24.
11. E. Rajanarendar, S. Ramakrishna, K. Govardhan Reddy, D. Nagaraju and Y. N. Reddy, *Bioorganic & medicinal chemistry letters*, 2013, **23**, 3954-3958.
12. G. S. Figueiredo, R. S. Zardo, B. V. Silva, F. A. Violante, A. C. Pinto and P. D. Fernandes, *Pharmacology, biochemistry, and behavior*, 2013, **103**, 431-439.
13. V. Jeankumar, R. Alokam, J. Sridevi, P. Suryadevara, S. Matikonda, S. Peddi, S. Sahithi, M. Alvala, P. Yogeeswari and D. Sriram, *Chemical Biology & Drug Design*, 2014, **83**, 498-506.
14. K. Kumar, M. Kamboj, K. Jain and D. Singh, *Spectrochimica Acta Part A: Molecular and Biomolecular Spectroscopy*, 2014, **128**, 243-247.
15. H. Ayalew, G. Reda, T. Gashaw, N. Babu and R. Upadhyay, *ISRN Organic Chemistry*, 2014, 894250.
16. A. A. Farag, *Drug research*, 2014, DOI: 10.1055/s-0034-1384609.
17. G. Bhaskar, Y. Arun, C. Balachandran, C. Saikumar and P. T. Perumal, *Eur J Med Chem*, 2012, **51**, 79-91.
18. X. M. Zhang, H. Guo, Z. S. Li, F. H. Song, W. M. Wang, H. Q. Dai, L. X. Zhang and J. G. Wang, *Eur J Med Chem*, 2015, **101**, 419-430.
19. Z. H. Chohan, H. Pervez, A. Rauf, K. M. Khan and C. T. Supuran, *Journal of enzyme inhibition and medicinal chemistry*, 2004, **19**, 417-423.
20. Y. Wang, F. Y. Chan, N. Sun, H. K. Lui, P. K. So, S. C. Yan, K. F. Chan, J. Chiou, S. Chen, R. Abagyan, Y. C. Leung and K. Y. Wong, *Chem Biol Drug Des*, 2014, DOI: 10.1111/cbdd.12361.
21. M. Majik, C. Rodrigues, S. Mascarenhas and L. D'Souza, *Bioorganic Chemistry*, 2014, **54**, 89-95.
22. D. J. Bauer, *British journal of experimental pathology*, 1955, **36**, 105-114.
23. A. B. da Silva, J. A. C. P. Gomes, E. D'Elia, M. J. C. Rezende, A. C. Pinto, B. N. M. Silva and B. V. Silva, *Int. J. Electrochem. Sci.*, 2013, **8**, 9317-9331.
24. H. Tahermansouri and F. Chitgar, *Journal of Chemistry*, 2013, **2013**, 1.
25. H. Pervez, N. Manzoor, M. Yaqub and K. M. Khan, *Journal of enzyme inhibition and medicinal chemistry*, 2014, **29**, 628-632.
26. A. Ali, S. Teoh, A. Salhin, N. Eltayeb, M. Ahamed and A. Majid, *Spectrochimica Acta Part A: Molecular and Biomolecular Spectroscopy*, 2014, **125**, 440-448.
27. A. Ali, S. Teoh, A. Salhin, N. Eltayeb, M. Ahamed and A. Majid, *Polyhedron*, 2014, **74**, 6-15.
28. D. Lamprou, J. Smith, T. Nevell, E. Barbu, C. Willis and J. Tsibouklis, *Journal of Advanced Microscopy Research*, 2010, **5**, 137-142.
29. R. Good and C. van Oss, in *Modern Approach to Wettability: Theory and Applications*, ed. S. M. a. L. G, Plenum, New York, 1992.
30. A. Muñoz-Bonilla, E. Ibarboure, E. Papon and J. Rodriguez-Hernandez, *Langmuir*, 2009, **25**, 6493-6499.
31. C. V. Cremmel, C. Zink, K. Maniura-Weber, L. Isa and N. D. Spencer, *Langmuir*, 2015, **31**, 8446-8452.
32. A. Bruinink, M. Bitar, M. Pleskova, P. Wick, H. F. Krug and K. Maniura-Weber, *Journal of biomedical materials research. Part A*, 2014, **102**, 275-294.
33. M. Srinivasarao, D. Collings, A. Philips and S. Patel, *Science*, 2001, **292**, 79-83.
34. A. Zhang, H. Bai and L. Li, *Chemical Reviews*, 2015, **115**, 9801-9868.
35. M. S. Park and J. K. Kim, *Langmuir*, 2004, **20**, 5347-5352.
36. X. Jiang, X. Zhou, Y. Zhang, T. Zhang, Z. Guo and N. Gu, *Langmuir*, 2010, **26**, 2477-2483.
37. X. Ran, K. Zhang, L. Shi, Z. Chi, W. Qiu and L. Guo, *RSC Advances*, 2015, **5**, 60518-60523.
38. C. C. Berry, G. Campbell, A. Spadiccino, M. Robertson and A. S. Curtis, *Biomaterials*, 2004, **25**, 5781-5788.
39. D. Beattie, K. H. Wong, C. Williams, L. A. Poole-Warren, T. P. Davis, C. Barner-Kowollik and M. H. Stenzel, *Biomacromolecules*, 2006, **7**, 1072-1082.
40. H. Li, Y. Jia, M. C. Du, J. B. Fei, J. Zhao, Y. Cui and J. B. Li, *Chem.-Eur. J.*, 2013, **19**, 5306-5313.
41. Y. D. Zhu, R. L. Sheng, T. Luo, H. Li, J. J. Sun, S. D. Chen, W. Y. Sun and A. Cao, *ACS applied materials & interfaces*, 2011, **3**, 2487-2495.
42. M. Gultekinoglu, Y. Tunc Sarisozen, C. Erdogdu, M. Sagiroglu, E. A. Aksoy, Y. J. Oh, P. Hinterdorfer and K. Ulubayram, *Acta Biomater*, 2015, **21**, 44-54.
43. R. Ron, D. Zbaida, I. Z. Kafka, R. Rosentsveig, I. Leibovitch and R. Tenne, *Nanoscale*, 2014, **6**, 5251-5259.
44. H.-B. Ahn, S.-J. Ahn, S.-J. Lee, T.-W. Kim and D.-S. Nahm, *American Journal of Orthodontics and Dentofacial Orthopedics*, 2009, **136**, 668-674.